The two-dimensional density of states in normal and superconducting compounds

P. Contreras, Anjna Devi, D. Uzcategui, E Ochoa

The two-dimensional density of states in normal and superconducting compounds.

P. Contreras [1,], Anjna Devi [2], D. Uzcátegui [1] and E. Ochoa [1]*

[1] Physics Departments, University of Los Andes, Mérida, 5001, Venezuela.
[2] Department of Physics, Government College Baroh, Kangra, Himachal Pradesh, India.
[*] Corresponding author pcontreras@ula.ve

Abstract

In this work, we present a review for the numerical calculation of the density of states (DOS) for two-dimensional tight-binding models with first neighbors in its normal state and for two superconducting order parameters. One is a singlet scalar state and the other is a triplet vector state. At the beginning an emphasis is given to the general expressions commonly used to the calculation of the density of states as the number of partial and total number of states, the degrees of freedom and the ab-initio methods most commonly used to its calculation. Then, the transition that happens to the normal states density of states by varying the Fermi energy and the hopping parameter is investigated. After that, the numerical calculation of the superconducting density of states using the zero temperature scattering cross-section is performed for the two order parameters. Finally, the residual density of states depending on disorder and the scattering potential strength using the Larkin equation are calculated for the two different in nature order parameter symmetries.

Keywords: Normal Density of States, Superconducting & Residual Density of States; Larkin Equation, Degrees of Freedom. Reduced Phase Space.

1. Introduction

The density of states (DOS) is a quantum mechanical concept derived from the total number of quantum states (Φ) with an energy less than a value E in a microscopic system, where Φ tells the total number of states & increases in energy with the DOS defined as $\rho(E) = {}^{d\,\Phi(\mathrm{E})}/_{d\,E}$. Also, the DOS can be derived within an small interval of energies δE as function of a reduced number of microscopic states (Ω) with the DOS being the proportionality coefficient in the relationship $\Omega(E) = \rho(E)\delta E$ where Ω is constant in energy [1]. On the other hand, the relation between the DOS and the degrees of freedom (f) states that the microscopic motion of a physical system that follows the Gibbs distribution (with a constant energy), the behavior of some particles is quasi-classical & happens only for some degrees of freedom. However, for the rest of degrees of freedom the motion is quantized and those degrees of freedom can be written as function of a quantum number (n) where the energy is quantized as $E_n(q, p)$ [2].

Additionally, the DOS can be function of external parameters (such as those of extensive type defined in statistical thermodynamics [1]) and in that case different degrees of freedom can be included in a macroscopic system. Thus, another way to derive the DOS comes from comparing the Gibbs distribution and the microcanonical ensemble in Statistical Mechanics [2]. It is more complicated to understand the derivation that includes the Planck constant ($2\pi\hbar$) and the relation with a volume in a hyperspace with one Planck constant for each pair of the conjugate variables q and p in phase space, where each microstate belongs to a $2fN$ - dimensional "hypercube", with a length $2\pi\hbar$ and a volume $(2\pi\hbar)^{fN}$[2].

In general, the DOS it is a measure of how many microscopic states are available to a system in a particular range of values of the energy. If the ground state energy for a physical system with N particles is given by $E_0 = f\,N\,\epsilon_0$, the energy difference from of an excited state from the ground state is represented by a general expression linking several parameters. Thus, $E - E_0 = fN(\langle\epsilon\rangle - \epsilon_0)$, where the notation indicates that $\langle\epsilon\rangle$ is the mean quantum energy per particle, ϵ_0 is the ground state energy of each particle, N is the number of particles, E & E_0 are the total energy and ground state energy of the N particles, and f are the degrees of freedom. This mean that the total number of states $\Phi(E - E_0) \sim \Phi(\langle\epsilon - \epsilon_0\rangle)^N \sim (\langle\epsilon\rangle - \epsilon_0)^N$ is a big number even for only one kind (f = 1) of degrees of freedom.

In solid-state physics, the DOS is expressed in terms of the system´s energy. As some authors point out [3], each element of volume/area in the phase space of position q and momenta p is replaced by a weighting factor in an energy integral, which is easier to work with at the quantum level. We make use of the rationalized Planck units ($\hbar = k_B =$

$c = 1$) to have a single unit of measurement, since it conducts to the conceptual framework of the reduced phase space for the zero temperature elastic scattering cross-section, that we have used previously in several works [4].

Thus, a DOS equation with equal number of spin up and down particles can be written as: 1st the sum of infinite delta functions; 2nd as the derivative of the total number of states; 3rd as a proportionality coefficient of the partial number of states, i.e., $N(\omega) = {}^{2}/_{V}\sum_{i}^{\infty}\delta(\omega - \omega_i) = {}^{d\,\Phi}/_{d\,\omega} \approx {}^{\Omega}/_{\delta\,\omega}$. The last two expressions relate the DOS and the number of total or partial states. An instructive interpretation of the DOS from a geometrical perspective is given in [3] where the DOS is defined as the slope between the number of macroscopically allowed quantum partial number of states (Ω) and an infinitesimal energy interval from ω to $\omega + \delta\omega$ in a two-dimensional space with variables (ω,Ω) [3].

The sum inside the delta function in momentum space, is adequate for the normal state DOS since disorder only changes the DOS value by a constant quantity. But in other cases as in unconventional superconductors is easy to replace the sum by a weighting factor into an energy integral, which is easier to deal with. Summarizing, the DOS is extensively used in applications to Statistical Mechanics, Solid State Physics, and Quantum Chemistry. Many, all ab-initio routines include the calculation of the DOS, and more important is that the DOS can be calculated not only for systems with N particles, but also for: 1st single molecules at the Hartree-Fock HF/6-311G* level [5] using the TDOS formalism [6]; 2nd dimer or trimer molecular systems with lack of inversion symmetry at the UDFT/B3LYP level [7], or in one and two-dimensional monolayers, such as nanowires and nanoflakes, where is clearly observed from several DOS calculations and their visualizations that the materials which are symmetrical for its up and down channels are non-magnetic and asymmetrical materials are magnetic in nature [8,9,10,11].

The structure of this work is as follows: In section 2 some details of the computational approach are outlined. In section 3, a detailed DOS calculation of the normal state with a tight binding model is performed. In section 4 the calculation of the superconducting DOS is performed for singlet and a triplet order parameters (OP). Finally, in section 4, the behavior of the residual density of states is addressed for both models using the formalism following the Larkin equation [12].

2. Computational details for the density of states with sums and Fermi averages.

For the numerical calculation of the DOS in the normal state, we make use an approximation of the Delta function using a 2D sum for momentum dependency with a δ function approximated by

$$N(E) \cong \sum_{kx,ky}\delta\left(E-\xi_{i,\boldsymbol{k}}\right) = \frac{1}{\pi}\sum_{kx,ky}\frac{n}{\left(E-\xi_{i,\boldsymbol{k}}\right)^{2}+n^{2}}, \quad (1)$$

where $\sum_{kx,ky}\delta\left(E-\xi_{i,\boldsymbol{k}}\right)$ is approximated by a Lorentzian 2D function. For the calculation of (1), it has been used a mess of $N \times N$ k-points with $N = \pm 400$ points. The other parameters in (1) are n = 0.005 that gives a well-defined delta function, and a dispersion TB law with first neighbors where two terms are responsible for the behavior of the DOS, i.e.,

$$\xi_{i,\boldsymbol{k}}(k_x,k_y) = \varepsilon_F + \xi_{hop}(k_x,k_y), \quad (2)$$

and where the $\boldsymbol{k}$ dependence is carried in the hoping term $\xi_{hop}(k_x,k_y)$ where t is the first neighbors coefficient, and thee function is given by

$$\xi_{hop}(k_x,k_y) = 2t\left[\cos\left({}^{k_x\pi}/_{N}\right) + \cos\left({}^{k_y\pi}/_{N}\right)\right]. \quad (2a)$$

On the other hand, for a superconductor with nonmagnetic impurity scattering it is used the equation which is derived from the Green function formalism (also known as T matrix formalism) [13,14] $N(\tilde{\omega}) = N_F\,\mathcal{R}[g(\tilde{\omega})]$ where $\mathcal{R}$ means the real part of the function $g(\tilde{\omega})$. The Fermi level DOS is N_F and the function containing the impurity effects is $g(\tilde{\omega}) = \left\langle \frac{\tilde{\omega}}{\sqrt{\tilde{\omega}^2-\Delta_0^2(k_x,k_y)}} \right\rangle_{FS}$ and has a zero superconducting energy gap parameter dependence. The function $g(\tilde{\omega})$ has the Fermi average $<\ldots>_{FS}$. This part requires a calculation that implies uncommon numerical routines to find from the zero self-consistent elastic scattering cross-section, the real and imaginary parts. The study of the zero temperature elastic scattering cross-section was firstly proposed in [15], and used with a specific disorder parametrization, i.e., the inverse dimensionless strength c and the impurity density Γ^{+} in [16] and references therein for isotropic Fermi surfaces.

Additionally, extended studies of the zero elastic scattering cross-section were recently performed in [17] to calculate $\widetilde{\omega}$ using two different numerical self-consistent routines for isotropic FS and a linear nodes OP with different c and Γ^{+} in order to establish differences in numerical routines. In [18] the work was performed for a linear nodes HTSC model using a tight binding parametrization for three different collisional regimes. For the for the Miyake Narikiyo quasi-nodes triplet OP [19], the tight-binding calculation of $\widetilde{\omega}$ was performed for ten values of the inverse strength parameter c showing that the cross-section is mostly in the unitary limit and few times in the intermedium limit [20].

In [21] the calculation was performed as function of the Fermi energy and it was distinguished the point nodes model from the quasi-nodal original model in the elastic scattering cross-section. In [22], the dependence on the zero temperature Δ_0 was modeled self-consistently for a triplet OP finding that the imaginary elastic scattering cross-section is always positive and fits well in the unitary limit. Finally, the quasi-nodal model was contrasted with the linear OP behavior by fixing the Fermi energy and the zero temperature superconducting gap in other to see the interplay between different kind of quasiparticles [23] in the elastic scattering cross-section [24,25].

If we are dealing with more than one Fermi surface sheet, the DOS is calculated according to equations such as $\frac{N(\omega)}{N_F} = p^{\gamma} N^{\gamma}\left(\frac{\omega}{\Delta_0^{\gamma}}\right) + p^{\alpha,\beta} N^{\alpha,\beta}\left(\frac{\omega}{\Delta_0^{\alpha,\beta}}\right)$ which is suitable for strontium ruthenate in a non-self-consistent way using a TB parametrization aiming at fitting experimental low-temperature data such as ultrasound attenuation in the superconducting state $\alpha(T)$ [26,27], the electronic superconducting thermal conductivity $\kappa(T)$ [28,29] and the electronic superconducting specific heat $C(T)$ [30,31] with relatively clean samples. Details of the original use of p^{γ} and $p^{\alpha/\beta}$ are found for the Sr_2RuO_4 normal state viscosity calculation in [32]. Other works of relevance for experimental fittings in strontium ruthenate are found in [33,34,35,36].

The equation used to calculate the DOS in dirty superconductors when taking into account the reduced phase space is the following [11]

$$\frac{N(\widetilde{\omega})}{N_F} = \langle \frac{\Re(\widetilde{\omega})}{\sqrt{2\,\rho_k}} \sqrt{1 + \frac{a_k}{\rho_k}} \rangle_{FS} + \langle \frac{\Im(\widetilde{\omega})}{\sqrt{2\,\rho_k}} \sqrt{1 - \frac{a_k}{\rho_k}} \rangle_{FS}, \quad (3)$$

where $\Re(\widetilde{\omega})$ & $\Im(\widetilde{\omega})$ are the coordinates in the reduced phase space, and the other symbols are $a_{\boldsymbol{k}} = \Re(\widetilde{\omega})^2 - \Im(\widetilde{\omega})^2 - \Delta_k^2$, $b = 2\,\Re(\widetilde{\omega})\,\Im(\widetilde{\omega})$, and $\rho_k = \sqrt{a_k^2 + b^2}$. Equation 3 is a very suitable, since it is directed related to the reduced phase space.

The tight-binding Fermi averages replacing the sum "$\sum_{kx,ky}(...)$" are performed using a weight in energy instead of the sum, i.e., $\sum_k^{\infty}(...) = \frac{1}{4\,\pi^2} \int \frac{d\,S_F}{|\overrightarrow{v_k}|} \int d\,E\,(...) = \langle \cdots \rangle_{FS}$ where E is the energy of the normal state, the Fermi velocity is given by the gradient $\overrightarrow{v_k} = grad\ E$, the surface $\boldsymbol{k}$-space element is expressed as $dS_F = \sqrt{d\,k_x^2 + d\,k_y^2}$, and the normal state density of states at the Fermi level is calculated by $N_F = \frac{1}{4\,\pi^2} \int \frac{d\,S_F}{|\overrightarrow{v_k}|}$ [37].

3. Normal state DOS and its evolution according to the Fermi energy:

In this section we present how the evolution of the density of states (DOS) can be numerically modeled by varying the Fermi energy parameter in (2). It is found in Fig. 1 that the implicit Fermi surface with $\xi_{i,\boldsymbol{k}}(k_x, k_y) = 0$ evolves from having a behavior with a mesh centered at (0,0) coordinates when the Fermi energy is negative and the hoping coefficient is positive, to a different behavior when both, the Fermi energy and the hoping parameter have positive values, and the Fermi surface for this case is centered in four pockets at the $\pm(N, N)$ corners. The values used for the model are given in Table 1.

Table 1: Evolution of the implicit Fermi surface for different sets of TB parameters

Fermi energy ε_F	*Hoping parameter t*	*Centered at N × N mesh points:*	$\xi_{i,k}(k_x, k_y) = 0$
-0.40 meV	+0.20 meV	$\pm(400,400)$	Red color
-0.04 meV	+0.20 meV	$\pm(400,400)$	Green color
+0.04 meV	+0.40 meV	(0,0)	Blue color
+0.40 meV	+0.40 meV	(0,0)	Yellow color

The implicit Fermi surface evolution in the N×N mesh is sketched in fig. 1, where are seen two well defined behaviors

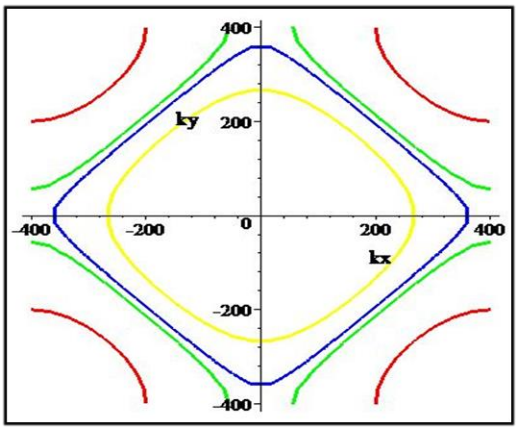

Figure 1: *The* $\xi_{i,k}(k_x, k_y) = 0$ *evolution in a 400×400 points mesh. The TB values for each color are given in table 1.*

following the values of the parameters in Table 1, two of the four implicit plots are centered at zero point (when the hoping parameter value is t = 0.20 meV, i.e. the green and red implicit plots). Meanwhile, the other two are centered at the corners of the square (when the hoping parameter value is t = + 0.40 meV, i.e. the yellow and blue implicit plots).

In addition, in this section, the normal density of states is calculated using (1) with the same parameters of Table 1 The results are presented in fig. 2

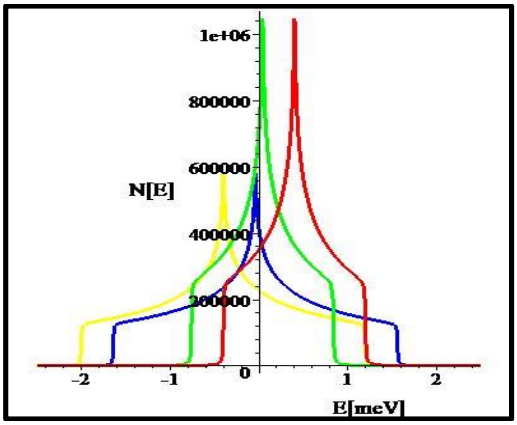

Figure 2: The density of states N(E) for 4 values of $\mathcal{E}_F$ *in a 400×400 points mesh. The TB values for each color are from table & fig. 1.*

As it can be seen from fig. 2, the density of states with Fermi energy values close to zero (blue & green colors) have almost an electron-hole symmetry behavior. Also those where the two tight binding coefficients have similar order of magnitude are less symmetric (yellow & red colors). If the hoping parameter is smaller as happen for the red and green cases, both centered at the corners, the DOS have more available quantum states than when the Fermi surface is centered at zero points. This is important and shows how the quantum behavior of those ceramics that have tight-binding parametrization (the red and green cases) (for example some HTSC in its normal state) present a more difficult quantum interpretation compared with the blue and yellow cases that mostly represent metallic alloys.

The drop to zero of the normal DOS can be understood in terms of a number of partial available quantum states constant as is has been explained in the introduction. Therefore, the DOS that is a coefficient of the partial number of

states Ω (see the introduction of this work) becomes negligible and probably other degrees of freedom start to play a more important role at those energies where N(E) drops to a zero value, meaning a constant number of partial states Ω.

4. Impurity superconducting DOS and its evolution as function of the scattering strength and disorder

In the superconducting state, we can compare two OP models. One, the 2D TB line nodes used to model the strontium doped lanthanum copper oxide superconductor with a $T_c \approx 44.35$ K for a polycrystalline sample [38,39,40] modeled with the parameters $t = 0.2$ meV, $\varepsilon_F = -0.4$ meV and $\Delta_0 = 33.9$ meV [41] shadowed gray in the 1st line of table 1. The linear nodes OP has even parity ***i*** that belongs to the irreducible representation B_{1g} of the D_{4h} point symmetry group [42,43].

The triplet case is represented in this section for the 2D γ-sheet Miyake Narikiyo quasi-point nodes model [12] for strontium ruthenate and $T_c \approx 1.5$ K for a bulk clean sample [44,45], with the values $t = 0.4$ meV, $\varepsilon_F = -0.4$ meV and $\Delta_0 = 1.0$ meV shadowed gray in the 4th line of Table 1. In this case the OP has odd parity ***i*** that belongs to the irreducible representation E_{2u} of the D_{4h} point symmetry group with GL coefficients *(1, i)* and 2D basis $(\sin(k_x), \sin(k_y))$ [19,46,47,48]. We would like to point out the intriguing 2D electronic nature of this material as is pointed out in [49].

In addition, to take into account the non-magnetic disorder effects in both order parameter models inside the superconducting DOS and the residual DOS, we use:

- The Born limit given by $\ell \boldsymbol{k}_F \gg 1$ or $\ell a^{-1} \gg 1$, where *l* is the mean free path, *a* is the lattice parameter, and $\boldsymbol{k}_F$ is the Fermi momentum.
- The intermediate scattering regime with $\ell \boldsymbol{k}_F \sim \ell a^{-1} > 1$.
- The unitary limit where holds that $\ell \boldsymbol{k}_F \sim \ell a^{-1} \sim 1$.

We use the parameter *c* which is inverse to the scattering strength U_0 to describe the dispersion limits for both OP numerical models. During the 70s & 80s, the formalism and some phenomenology of the physics for non-magnetic impurity scattering in normal metals and alloys were described in [50] from a work firstly proposed by Edwards [51]. In monography [52] it was noticed that in studying metallic alloys, there are singularities in the DOS for disordered systems such as those involving nonmagnetic impurities, or stoichiometric nonmagnetic atomic potentials U_0, they pointed out that keeping a 1st power in impurity concentration suffixes the calculation. We consider also instructive to mention that the ARPES technique is related to a fundamental equation *"the Fermi Golden Rule"*. A robust introduction to ARPES can be found in [53].

5. Numerical results for the self-consistent DOS with non-magnetic disorder

Figure 3 shows the density of states DOS, calculated numerically using (3) that includes the zero elastic scattering cross-section reduced phase space. The resulting plot is the density of states $N(\tilde{\omega})/N_F$ as a function of the normalized frequency ω/Δ_0. In the clean limit (without impurities), the parameter for the concentration of disorder Γ^+ is normalized by the zero energy gap and denoted as $\zeta = \Gamma^+/\Delta_0$. It is observed that, there are no dressed fermionic quasiparticles if there is no disorder. Thus, the number of occupied states starts to grow linearly, since it represents a nodal line OP [42] until an energy value equal to that of the zero superconducting gap is reached. At $\omega = \Delta_0$, there is a drastic change in slope that resembles on the right side the shape of a BCS superconductor [54], where the DOS presents a singularity for $\omega = \Delta_0$ and is zero below the gap, the other type of suppression in superconducting states (when there are magnetic impurities) is explained following a physical kinetic analysis in [55].

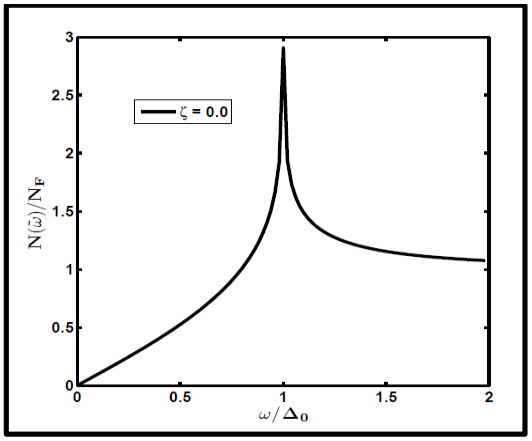

Figure 3. Superconducting density of states (DOS) for a tight binding line nodes OP if $\zeta = 0$. There aren't residual states at zero energy.

Figure 4 shows five curves calculated for the values of disorder with $\zeta = 0.001, 0.005, 0.010, 0.015, 0.020$ in the unitary limit when c = 0. However, at zero frequency, it is observed that there is a residual density of states for all 5 values of ζ, which is a consequence of the presence of nonmagnetic impurities in the reduced phase space for the line nodes model, which behavior is modified by the inverse scattering lifetime. It is noticed that a higher concentration of impurities, the amount of states at the frequency value ω = 0.0 meV is also higher.

The residual normalized DOS is bigger for the thinner line ($\zeta = 0.020$) compared to other four curves, the thicker line ($\zeta = 0.001$) has still a considerable amount of residual DOS.

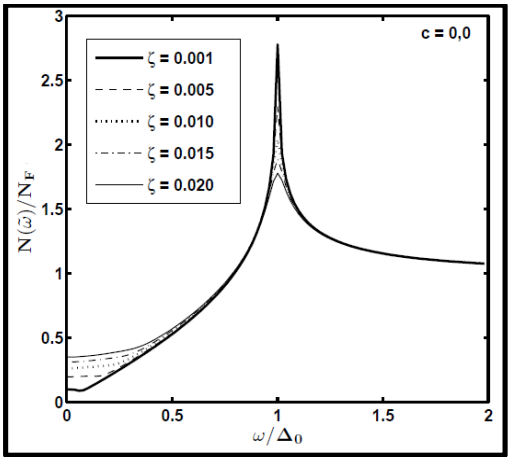

Figure 4. Superconducting DOS for a lines nodes OP. The residual DOS shows significant dressed quantum levels at zero energy due to the strong scattering potential.

Figure 5, shows the superconducting DOS for a weaker scattering potential with c = 0.4 and the disorder parameter $\zeta = 0.001, 0.005, 0.010, 0.015, 0.020$. The strength when c = 0.4 was established numerically from the analysis of the zero temperature elastic scattering cross-section as the Born limit for a linear OP [18]. However, in this case the residual $^{N(0)}/_{N_F}$ weakly increases as ζ increases and it is noticeably smaller compared to the $^{N(0)}/_{N_F}$ values in fig. 2 that corresponds to the unitary limit, where there is a strong elastic scattering, suggesting that a strong nonmagnetic dispersion potential produces more occupied states, than weaker scattering potentials at zero energy.

This can be defined as the signature for the unitary state in the residual DOS analysis compare with the nonlocal minimum observed in the analysis of the imaginary part of the elastic cross-section $\Im\,[\tilde{\omega}]\,(\omega + i\,0^{+})$ [18].

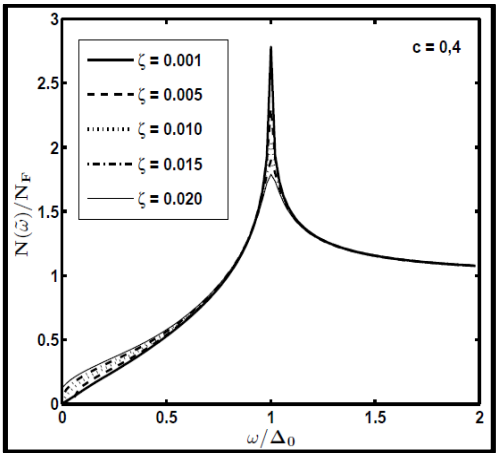

Figure 5. The DOS for the nodal line OP in strontium doped lanthanum compound with 5 disorder values. The residual density is small when compared to fig. 4. There are only a few quantum states available in the hydrodynamic limit.

The next calculation is performed for the γ sheet of the triplet superconductor strontium ruthenate with an OP that belongs to the irrep E_{2u} of the D_{4h} point group. Figure 6 shows six curves calculated for different values of the normalized disorder $\zeta = \Gamma^{+}/\Delta_0$. The simulation was performed for $\zeta = 0.00, 0.01, 0.02, 0.03, 0.10, 0.20$ in the unitary limit when the inverse elastic scattering parameter $c = 0$ since according to the analysis [19, 44, 45, 46, 47, 48, 49]. Triplet OP are suitable to analyze in this limit due to strong nonmagnetic strontium potential. A contrast concerning the previous case drawn in Figures 3 - 5 is that the dimensionless disorder parameter for the triplet case is one order of magnitude bigger than the dimensionless singlet OP.

This is partially explained because the γ-sheet uses an experimental zero gap value $\Delta_0 = 1.0$ meV, that is an order of magnitude smaller that the lines nodes OP with a zero gap $\Delta_0 = 33.9$ meV, and therefore the triplet case has a smaller reduced phase space for scattering events. Additionally, in the triplet compound, *Sr* atoms are located in the lattice with an additional nonmagnetic impurity level in the energy zone. Thus, *Sr* atoms are part of the D_{4h} tetragonal structure and also are the scattering centers, that explains the stronger pair breaking mechanism and the additional impurity level.

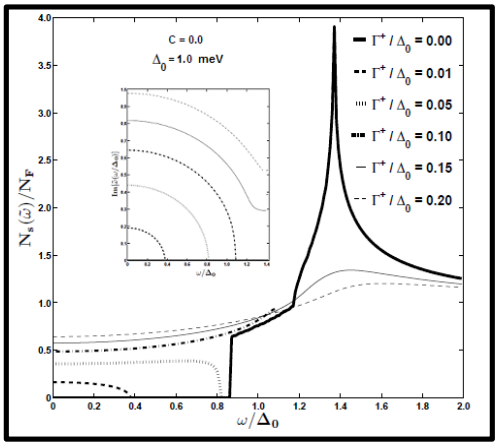

Figure 6. DOS for the quasi-point nodes with 6 values of nonmagnetic impurity doping including the clean case Residual N(0) is found for 5 non-zero ζ values. The tiny MN gap is found for ζ = 0.05.

Figure 6 shows that in the absence of impurity levels (black line where $\zeta = 0.00$), we do not observe non zero values for the density $N(\tilde{\omega})/N_F$ as happens for BCS superconductors [54]. It means that when doing calculations that involved triplet states and scattering is excluded, there is no pair breaking effects and bosonic quasiparticles dominate the behavior below the transition temperature. It occurs numerically below 0.83 meV in this calculation. Generally speaking, this value depends on the choice of the TB parameters, i.e., how close will be the Fermi surface to the zero gap Δ_0 value in the MN model. We have used parameters from the 4th column in Table 1 (shadowed gray) to calculate the DOS.

For a parameter value of $\zeta = 0.01$, we observe still an intermedia well-formed BCS gap, from frequencies in the interval (0.4,0.83) meV, and with a small quantity of quantum states at low frequencies due to strong scattering that happens in the unitary regime when the reduced phase space is activated with a nonzero imaginary part of the cross-section, and the mean free path ℓ is comparable to the magnitude of the inverse Fermi length $|\boldsymbol{k}_F|^{-1}$, or to the value of the

lattice parameter a. To illustrate what happens numerically we show in the insert on the upper left side of fig. 6, the reduced phase space calculation, and it is observed the following: for the $\zeta = 0.01$ case, the imaginary part of the cross-section dies inside of the superconducting phase. Therefore, it does not become a normal metal and could be a signature of an antiferromagnetic state as happens to the antiferromagnetic insulator LaCuO [39].

For impurity values $\zeta = 0.05$ it agrees with an inhomogeneous phase that is the Miyake-Narikiyo tiny gap inside of which there are not fermionic quantum levels. Henceforth, the tiny Miyake-Narikiyo tiny gap predicted and used to explain microscopically the behavior of triplet pairing superconductors such as strontium ruthenate [19], is observed in fig. 6 for a impurity value $\zeta = 0.05$ as was also observed in [20,21,22] using the imaginary part analysis of the scattering cross-section $\Im\,[\widetilde{\omega}]\ (\omega + i\,0^{+})$. The DOS calculation also agrees with [20] in the sense that only the unitary limit persists in Sr_2RuO_4. It is noticed that a higher concentration of impurity levels given by the values $\zeta = 0.10, 0.15, 0.20$, the number of occupied quantum states at both, low and high frequencies increase, that is a consequence of having an increasing reduced phase space and therefore more possibilities for scattering events, but is still small compare with the HTSC nodal lines OP case [24].

Therefore, For the values of the disorder parameter $\zeta = 0.10,\ 0.15, 0.20$, there are normal state DOS levels available, and the peak at ω = 1.4 meV considerable reduces with a tendency where $N(\omega) \sim N_F$ above T_c. Therefore, in the superconducting triplet model, we observe two phases, one tiny phase (the MN gap) without electronic levels (BCS type) and another with normal-state dressed quantum levels, contrasting with the strontium substitute lanthanum cuprate calculation, where dressed fermionic levels are found.

5. Numerical results for the residual density of states and the pair breaking

The residual equation for the density of states is theoretically obtained by setting up the real frequency as an imaginary number, i.e., $\omega = i\,\alpha$ in (4). Thus, $\widetilde{\omega} = \omega + i\,\alpha$, with α a new disorder parameter ($0 \leq \alpha \leq 1$). This does not require a self-consistent routine, but it needs a fixed point numerical calculation. In such a case, we get the following general equation for the residual density of states ($^{N(0)}/_{N_F}$) with a new dimensionless disorder parameter $C_0 = \frac{\alpha}{\Delta_0}$

$$N(0) = N_F \left\langle \frac{C_0}{\sqrt{C_0^2 + \Delta_0^2(k_x, k_y)}} \right\rangle_{FS}. \quad (4)$$

where (4) depends on the symmetry of the OP, the elastic scattering regime of the imaginary part of the zero temperature elastic scattering cross-section, i.e., unitary, intermedia and Born cases; and finally also depends on the Fermi surface average, so we can control the residual DOS the same way as we did for the zero temperature elastic scattering cross-section and the superconducting density of states.

The functional dependence $\frac{T_c}{T_{c0}} = f\left(\frac{N(0)}{N_F}\right)$, where T_{co} indicates the transition temperature without disorder and T_c the transition temperature including disorder is the Larkin equation [] for suppression of impurity states in the case of nonmagnetic disorder, when the critical temperature T_c decreases as a function of the pair breaking parameter η_c,

$$\ln\frac{T_c}{T_{c0}} = \psi\left(\frac{1}{2}\right) - \psi\left(\frac{1}{2} + \eta_c\right) = \psi'\left(\frac{1}{2}\right)\frac{\Gamma^{+}}{2\pi T_c}. \quad (5)$$

In (5) the superconducting pair breaking parameter is defined as $\eta_c = -\frac{4\,\pi}{1.764}\ln\frac{T_c}{T_{c0}}$, were T_{c0} is the transition temperature for a clean superconductor ($\alpha = 0$), T_c represents the transition temperature for dirty superconductors, i.e., $\alpha \neq 0$, $\psi(x)$ is the digamma function, and $\psi'(x)$ is the derivative of the digamma function. Table 2 summarizes the expression that can be obtained if the tight binding approximation is accounted for and they do not differentiate from the isotropic case with angular dependence of the Fermi surface.

The analytical expressions for the calculation of the relationship $\frac{T_c}{T_{c0}} = f\left(\frac{N(0)}{N_F}\right)$, for the cases that we plot in this section can be obtained after some long algebraic manipulations using equations (7) and (8). The difference with previous works [56,57] is that the Fermi surface average depends on more parameters $\langle\ldots\rangle_{FS}$, the basis function ϕ_k in the case of a scalar line nodes OP, and the complex triplet vector OP $\boldsymbol{d_k}$ are the same used for the density of states calculation in the previous paragraph, the tight binding parameters are those shadowed gray in Table 1. A discussion with second and third harmonics for the triple OP is given in Miyake-Narikiyo original work [19].

Theoretically it is known that nonmagnetic impurities destroy superconductivity in unconventional superconductors [12,57] and reduce the value of the transition temperature T_{c0}. The residual DOS changes as a function of T_c, as it is shown accordingly to Table 2. Noticeable in this work is that the parameter C_0 depends on the Fermi surface averages. In order to numerically evaluate the polynomic expressions involved, it is more convenient to simplify the analysis to the three cases: The Born, intermedia and unitary scattering regimes (see Table 2 for a summary of the equations involved).

Table 2: C_0 parameter & residual DOS; summarized for both irrep, B_{1g} and E_{2u} and the scattering limits.

Residual Density of states RDOS TB formalism	***Expressions for C_0 in the Born and intermedia limits***	***Expressions for C_0 in the unitary limit***	***Residual DOS for Born & intermedia regimes***	***Residual DOS for the Unitary limit***
Singlet parity linear nodes OP	$C_0 = \pi\eta_c \langle \frac{\sqrt{C_0^2 + \phi_k^2}}{C_0} \rangle_{FS}^{-1}$	$C_0 = \pi\eta_c \langle \frac{\sqrt{C_0^2 + \phi_k^2}}{C_0} \rangle_{FS}$	$\frac{N(0)}{N_F} = \frac{C_0}{\pi\eta_c}$	$\frac{N(0)}{N_F} = (\frac{C_0}{\pi\eta_c})^{-1}$
Triplet parity quasi-point nodes OP	$C_0 = \pi\eta_c \langle \frac{\sqrt{C_0^2 + \lvert \boldsymbol{d}_k^2 \rvert}}{C_0} \rangle_{FS}^{-1}$	$C_0 = \pi\eta_c \langle \frac{\sqrt{C_0^2 + \lvert \boldsymbol{d}_k^2 \rvert}}{C_0} \rangle_{FS}$	$\frac{N(0)}{N_F} = \frac{C_0}{\pi\eta_c}$	$\frac{N(0)}{N_F} = (\frac{C_0}{\pi\eta_c})^{-1}$

The results of the numerical calculation using equations taken from Table 1 are shown in fig. 7 for the case of linear nodes OP. At zero T_c/T_{c0} the largest residual DOS value for both cases is obtained (for unitary and Born limits). On the other hand, as $N(0)/N_F$ increases, T_c/T_{c0} ratio falls to zero, faster for a weak scattering Born non-magnetic potential limit than for the unitary case. In addition, from Figure 5, we see that the unitary limit presents a curve that always has the same sign in slope; meanwhile the Born limit changes it signs and even has a linear behavior dependence for $N(0) \sim \frac{1}{2} N_F$.

Figure 8 compares the unitary limit of the OP used with measurements taken from specific heat in the compound strontium doped lanthanum ceramic for different experimental values of strontium doped obtained experimentally [56]. Strontium doping has been extensively studied in the cuprate $La_{2-x}Sr_xCuO_4$ for smaller orders of strontium concentration [41,56]. The color points with the impurity atoms are from values of specific electronic heat capacity *C(T)* in the superconducting state, where in Figure 6 the gray color corresponds to x = 0.10, green color corresponds to x = 0.18, blue color corresponds to x = 0.20, and red color corresponds to x = 0.22 [56]. We see a tendency for the experimental red points with x = 0.22 corresponding to our reduced value ζ = 0.020 in correspondence with both the unitary theoretical residual density of states and the self-consistent unitary case of the previous section (fig. 4) .

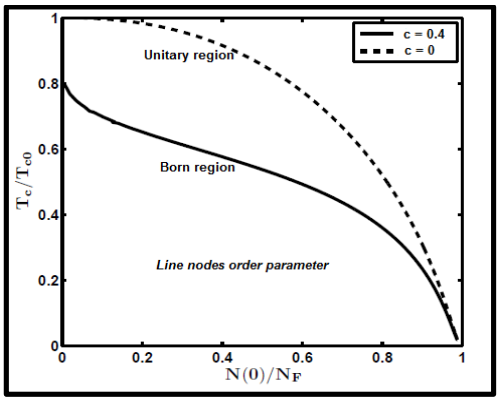

Figure 7. Numerical calculation of the residual density of states in the case of the singlet line nodes in the Born, and the unitary limits following equations in Table 1.

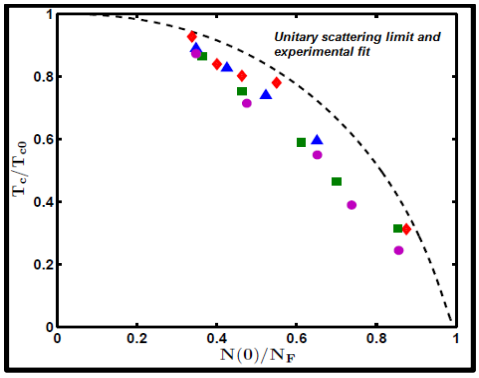

Figure 8. Fits of residual DOS for the unitary limit with data from $La_{2-x}Sr_xCuO_4$ [45]. Different colors correspond to different hopping parameters.

In fig. 9, $\frac{T_c}{T_{c0}}$ falls to zero slowly if the fixed point calculation is done for the unitary limit. As in the case of line nodes. Meanwhile, the unitary triplet OP presents a curve that always has the same shape and slope; the intermediate limit changes its slope weaker, slightly contrasting with the OP nodal line situation in fig. 7, where there are intermediate scattering events. Fig. 9, also compares the unitary limit of the triplet OP and experimental values the compound strontium ruthenate [19,30]. In this case we recall that strontium atoms add an additional impurity level since they are part of the crystal structure. The tight binding calculation in this case confirms the MN [19] original results.

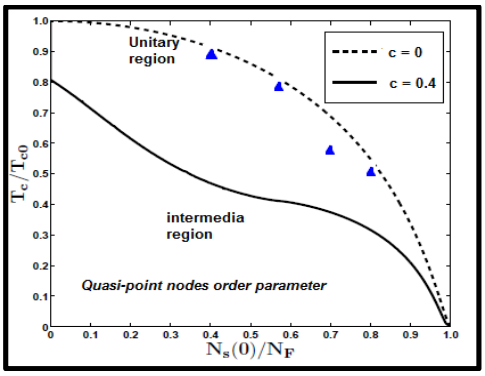

Figure 9. Numerical calculation of the residual DOS for the triplet OP in intermedia and unitary limits. The blue color shows the experimental fits corresponding to Sr_2CuO_4 [36,46].

6. *Conclusions & Recommendations*

This work was aimed at revisiting the calculation of the density of states and the residual with frequency values taken from a self-consistent calculation of the real & imaginary parts of the elastic scattering cross-section with a tight binding framework and for two order parameter models. The strontium-substituted lanthanum cuprate line nodes case [42], and strontium ruthenate symmetry breaking triplet model [19], where the density of state levels come from calculations in the reduced phase space when non-magnetic pair breaking disorder destroys superconductivity. Self-consistent calculations are in general very computing demanding as stated in [58].

Section 1 was aimed ad briefly review main concepts and the importance of the density of states in ab-initio calculations for novel materials. Section 2 the details of the computational approach were outlined. In section 3 a detailed density of states calculation of the normal state with a tight binding model was performed and interpreted in terms of the degrees of freedom. Section 4 the calculation of the superconducting density of states was self-consistently performed for singlet and a triplet OP using the zero temperature elastic cross-section for three scattering regimes. Finally, in section 4, the behavior of the residual density of states was addressed for both models using the formalism following the Larkin equation [12].

It is also recommended to use the tight-binding and other ab-initio frameworks to the study of numerical simulations as the density of states & other physical properties in novel unconventional superconductors with different nature as recently as has been done in several works [18,21,22,59,60,61] and references therein.

7. Acknowledgements

This research did not receive any specific grant from funding agencies in the public, commercial, or not-for-profit sectors. We acknowledge discussions about the presentation of the results with D. Osorio.

8. References

[1] Reif, F. (1965). Fundamentals of Statistical and Thermal Physics. McGraw-Hill.

[2] Landau, L. & Lifshitz, E. (1980). Statistical Physics. Pergamon Press.

[3] Mulhall, D. & Moelter, M. (2014). Calculating and visualizing the density of states for simple quantum mechanical systems. American Journal of Physics. 82(7):665-673. DOI: 10.1119/1.4867489

[4] Contreras, P. & Osorio, D. (2023). A Tale of the Scattering Lifetime and the Mean Free Path. arXiv:2301.05322 [cond-mat.supr-con] DOI: 10.48550/arXiv.2301.05322

[5] Contreras, P., Seijas L. &, Osorio D. (2021). TDOS quantum mechanical visual analysis for single molecules. Canadian Journal of Pure and Applied Sciences. Vol. 15(2), 5239 ISSN: 1920-3853

[6] Lu, T. and Chen, F. 2012. Multiwfn: A multifunctional wave function analyzer. Journal of Computational Chemistry. 33(5):580-592. DOI: 10.1002/jcc.22885

[7] Burgos, J., Seijas, L., Contreras, P. and Almeida, R. (2017). On the geometric and magnetic properties of the monomer, dimer and trimer of NiFe2O4. Journal of Computational Methods in Sciences and Engineering. 17(1):19. DOI: 10.3233/JCM-160657

[8] Devi A, Kumar A, Ahluwalia P.K, Singh A., "Novel properties of transition metal dichalcogenides monolayers and nanoribbons (MX2, where M = Cr, Mo, W and X = S, Se): A spin resolved study", Materials Science and Engineering: B, 2021; 271: 115237. DOI: 10.1016/j.mseb.2021.115237

[9] Devi A., Kumar N., Thakur A., Kumar A., Singh A., and Ahluwalia P. K., "Electronic band gap tuning and calculation of mechanical strength & deformation potential by applying uniaxial strain on MX2 (M=Cr, Mo, W & X= S, Se) monolayers and nanoribbons", ACS Omega, 2022; 7(44), 40054-40066. DOI: 10.1021/acsomega.2c04763

[10] Devi A., Kumar A, Singh A. and Ahluwalia P. K, "A comparative study on phonon spectrum and thermal properties of graphene, silicene and phosphorene", AIP Conference Proceedings, 2019; 2115, 030386. DOI: 10.1063/5.0016612

[11] Devi A, Kumar A, Kumar T, Bharti, Adhikari R, Ahluwalia P.K, Singh A., "Structural, electronic and magnetic properties of CrMSn and CrMSeN nanoflakes: An ab initio Investigation", Physica E: Low-dimensional Systems and Nanostructures.2021; 134: 114825. DOI: 10.1016/j.physe.2021.114825

[12] Larkin, A. (1965). Vector pairing in superconductors of small dimensions. JETP Letters. Vol. 2(5), 105. ISSN: 0370-274X

[13] Mineev, V. & Samokhin, K. (1999). Introduction to Unconventional Superconductivity. Gordon and Breach Science Publishers.

[14] Hussey, N. (2002). Low-energy quasiparticles in High-Tc cuprates, Adv. in Phys, 51:8, 1685. DOI: 10.1080/00018730210164638

[15] Pethick, C. & Pines, D. (1986). Transport processes in heavy-fermion superconductors. Phys. Rev. Lett. 57(1), 118, DOI: 10.1103/PhysRevLett.57.118

[16] Schachinger, E. & Carbotte, J. (2003). Residual absorption at zero temperature in d-wave superconductors. Phys. Rev. B 67, 134509. DOI: 10.1103/PhysRevB.67.134509

[17] Contreras, P. & Moreno, J. (2019). A non-linear minimization calculation of the renormalized frequency in dirty d-wave superconductors. Canadian Journal of Pure and Applied Sciences. Vol. 13(2), 4765 ISSN: 1920-3853

[18] Contreras, P. & Osorio, D. (2021) Scattering Due to Non-magnetic Disorder in 2D Anisotropic d-wave High Tc Superconductors. Engineering Physics 5, 1, DOI: 10.11648/j.ep.20210501.11

[19] Miyake, K. & Narikiyo, O. (1999). Model for Unconventional Superconductivity of Sr_2RuO_4. Effect of Impurity Scattering on Time-Reversal Breaking Triplet Pairing with a Tiny Gap. Phys. Rev. Lett. 83, 1423. DOI: 10.1103/PhysRevLett.83.1423

[20] Contreras, P., Osorio, D. & Ramazanov, S. (2022). Nonmagnetic tight- binding effects on the γ-sheet of Sr_2RuO_2. Rev. Mex. Fis. 68 (2) 1, DOI: 10.31349/RevMexFis.68.020502

[21] Contreras, P., Osorio, D. & Tsuchiya, S. (2022) Quasi-point versus point nodes in Sr_2RuO_2, the case of a flat tight binding γ sheet. Rev. Mex. Fis 68(6), 060501 1–8. DOI: 10.31349/RevMexFis.68.060501

[22] Contreras, P., Osorio, D. & Devi, A. (2022). The effect of nonmagnetic disorder in the superconducting energy gap of strontium ruthenate, Physica B: Condensed Matter. Vol. 646, 414330. DOI: 10.1016/j.physb.2022.414330

[23] Kaganov, M. & Lifshitz, I. (1989). Quasiparticles: Ideas and Principles of Quantum Solid State Physics. 2nd edition. Moscow "Nauka".

[24] Contreras, P. Osorio, D. & Beliayev, E. (2022) Dressed behavior of the quasiparticles lifetime in the unitary limit of two unconventional superconductors. Low Temp. Phys. 48, 187. DOI: 10.1063/10.0009535

[25] Contreras, P. Osorio, D. & Beliayev, E. (2022) Tight-Binding Superconducting Phases in the Unconventional Compounds Strontium-Substituted Lanthanum Cuprate and Strontium Ruthenate. American Journal of Modern Physics. Vol. 11(2) 32, DOI: 10.11648/j.ajmp.20221102.13

[26] Lupien, C. MacFarlane, W., Proust, C., Taillefer, L., Mao, Z. & Maeno, Y. (2001) Ultrasound Attenuation in Sr_2RuO_4: An Angle-Resolved Study of the Superconducting Gap Function, Phys. Rev. Lett. 86: 5986 DOI: 10.1103/PhysRevLett.86.5986

[27] Contreras, P., Walker, M. B. & Samokhin, K. (2004). Determining the superconducting gap structure in Sr_2RuO_4 from sound attenuation studies below T_c. Phys. Rev. B, 70:184528. DOI: 10.1103/PhysRevB.70.184528

[28] Tanatar, M., et al. (2001). Thermal conductivity of superconducting Sr_2RuO_4 in oriented magnetic fields. Phys. Rev. B 63: 064505 DOI: 10.1103/PhysRevB.63.064505

[29] Contreras, P. (2011). Electronic heat transport for a multiband superconducting gap in Sr_2RuO_4. Rev. Mex. Fis. 57(5) 395.

[30] Nishizaki, S., Maeno, Y. Farner, S. Ikeda, S. & Fujita, T. (1998) Evidence for Unconventional Superconductivity of Sr_2RuO_4 from Specific-Heat Measurements. Journal of the Physical Society of Japan, 67, 560 DOI: 10.1143/JPSJ.67.560

[31] Contreras, P. et al., (2014). A numerical calculation of the electronic specific heat for the compound Sr_2RuO_4 below its superconducting transition temperature. Rev. Mex. Fis. 60(3), 184.

[32] Walker, M. B., Smith, M. & Samokhin, K. (2001) Electron phonon interaction and ultrasonic attenuation in the ruthenate and cuprate superconductors Phys. Rev. B, 65: 014517 DOI: 10.1103/PhysRevB.65.014517

[33] Nomura, T. (2005). Theory of transport properties in the p-wave superconducting state of Sr_2RuO_4 - a microscopic determination of the gap structure. Journal of the Physical Society of Japan. 74(6):1818-1829. DOI: 10.1143/jpsj.74.1818

[34] Taniguchi, H., Nishimura, K., Goh, S., Yonezawa, S. & Maeno, Y. (2015). Higher-Tc superconducting phase in Sr_2RuO_4 induced by in-plane uniaxial pressure. Journal of the Physical Society of Japan. 84(1):014707. DOI: 10.7566/JPSJ.84.014707

[35] Wu, W. & Joynt, R. (2001). Transport and the order parameter of superconducting Sr_2RuO_4. Physical Review B. 64(10):100507(R). DOI: 10.1103/PhysRevB.64.100507

[36] Zhitomirsky, M. & Rice, T. (2001). Interband proximity effect and nodes of superconducting gap in Sr_2RuO_4. Phys. Rev. Lett. 87, 057001. DOI: 10.1103/PhysRevLett.87.057001

[37] Ashcroft, N. & Mermin, D. (1976) Holt, Rinehart and Winston. New York. ISBN: 978-0-030-83993-1

[38] Bednorz, J. & Müller. K. (1986). Possible high T_c superconductivity in the *BaLaCuO* system. Z. Physik B - Condensed Matter 64, 189–193. DOI: 10.1007/BF01303701

[39] Kastner, M., Birgeneau, R., Shirane, G. & Endoh, Y. (1998). Magnetic, transport, and optical properties of mono layer copper oxides Rev. Mod. Phys. 70, 897. DOI: 10.1103/RevModPhys.70.89

[40] Xiao, G. Streitz, F., Gavrin, Du, A. & Chien C. (1987). Effect of transition-metal elements on the superconductivity of Y-Ba-Cu-O, Phys. Rev. B.85(16), 8782. DOI: 10.1103/PhysRevB.35.8782

[41] Yoshida, T. et al. (2012). Pseudogap, Superconducting Gap, and Fermi Arc in High-Tc Cuprates Revealed by Angle-Resolved Photoemission Spectroscopy. Journal of the Physical Society of Japan, 81:011006, DOI: 10.1143/JPSJ.81.011006

[42] Scalapino, D. (1995). The case for d_{x2-y2} pairing in the cuprate superconductors. Physics Reports. 1995. 250(6):329-365 DOI: 10.1016/0370-1573(94)00086-I

[43] Tsuei, C. & Kirtley, J. (2000). Pairing symmetry in cuprate superconductors. Reviews of Modern Physics, 72:969 DOI: 10.1103/RevModPhys.72.969

[44] Maeno, Y., et al. (1994) Superconductivity in a layered perovskite without copper. Nature (London). 372:532. DOI: 10.1038/372532a0

[45] Rice, T. & Sigrist, M. (1995) Sr_2RuO_4: an electronic analogue of 3He? Journal of Physics: Condensed Matter. 7(47) L643-L648.

[46] Walker M. B. & Contreras, P. (2002). Theory of elastic properties of Sr_2RuO_4 at the superconducting transition temperature. Physical Review B. 66 (21): 214508. DOI: 10.1103/PhysRevB.66.214508

[47] Sigrist, M. (2002) Ehrenfest relations for ultrasound absorption in Sr_2RuO_4, J. Phys. Soc. Japan 107(5) 917.

[48] Contreras, P. et al., (2016) Symmetry Field Breaking Effects in Sr_2RuO_4, Rev. Mex. Fis. 62(5) 442.

[49] Maeno, Y. Yoshida, K. & Hashimoto, H. (1997). Two-dimensional Fermi liquid behavior of the superconductor Sr_2RuO_4. Journal of the Physical Society of Japan, 66(5), 1405. DOI: 10.1143/JPSJ.66.1405

[50] J. M. Ziman. 1979. Models of Disorder: The Theoretical Physics of Homogeneously Disordered Systems 1st Edition, Cambridge.

[51] Edwards, S. F. (1958). A new method for the evaluation of electric conductivity in metals, Philosophical Magazine, 3(33) 1020. DOI: 10.1080/14786435808243244

[52] Lifshitz, I., Gredeskul, S. & Pastur, L: (1988). Introduction to the theory of disordered systems. John Wiley and Sons.

[53] A. Palczewski. 2010. Angle-resolved photoemission spectroscopy (ARPES) studies of cuprate superconductors. Ph. D. Graduate Theses and Dissertations. Paper 11641. Physics CC commons repository

[54] Bardeen, J., Cooper, L. & Schrieffer, J. (1957). Microscopic Theory of Superconductivity, Phys. Rev. 106(1), 162. DOI: 10.1103/PhysRev.106.162

[55] Ambegaokar, V. & Griffin, A. (1965) Theory of the Thermal Conductivity of Superconducting Alloys with Paramagnetic Impurities, Phys. Rev. 137(4A), A1151. DOI: 10.1103/PhysRev.137.A1151

[56] Momono, M. & Ido, M. (1996) Evidence for nodes in the superconducting gap of $La_{2-x}Sr_xCuO_4$. T^2 dependence of electronic specific heat and impurity effects, Physica C 264, 311, DOI: 10.1016/0921-4534(96)00290-0

[57] Sun, Y. & Maki, K. (1995). Transport Properties of D-Wave Superconductors with Impurities, EPL 32, 355.

[58] Jansen, R., Farid, B. & Kelly, M. (1991) The steady-state self-consistent solution to the nonlinear Wigner-function equation; A new approach. Physica B Condensed Matter 175(1-3):49-53. DOI: 10.1016/0921-4526(91)90688-B

[59] Kasen S. (2020). Response functions of strongly correlated electron systems: From perturbative to many-body techniques. Ph. D. Graduate Thesis.

[60] Photopoulos, R. & Frésard, R. (2019), Cuprate Superconductors: A 3D Tight-Binding Model for La-Based Cuprate Superconductors Ann. Phys. 531, 1970044. DOI: 10.1002/andp.201970044

[61] Kang B. L. et al. (2022) NMR Evidence for Universal Pseudogap Behavior in Quasi-Two-Dimensional FeSe-Based Superconductor, Chin. Phys. Lett. Vol. 39(12), 127401 DOI: 10.1088/0256-307X/39/12/127401